# 2519 高强铝合金双丝 GMAW 焊接工艺

范成磊[1,2]， 梁迎春[2]， 杨春利[1]， 程士军[1]
（1 哈尔滨工业大学 现代焊接生产技术国家重点实验室，哈尔滨 150001
2 哈尔滨工业大学 机械工程博士后流动站）

摘 要：针对 20 mm 厚 2519 铝合金板，试验了大电流两道焊（DL）和小电流四道焊（XS）两种 GMAW 焊接工艺对焊缝成形和接头的力学性能的影响。结果表明，DL 和 XS 焊接接头的抗拉强度都不足母材的 60%，但 DL 接头的抗拉强度和伸长率比 XS 高而冲击韧度比 XS 低。综合 DL 和 XS 焊接工艺的优点，提出了新的大电流四道焊接工艺（DS）。对接头的力学性能测试表明，DS 焊接接头抗拉强度达到母材的 61.2%，冲击韧度较 DL 焊接接头有所提升。DS 焊缝区组织主要是 α 相和弥散分布的共晶组织；对接头进行硬度测试发现，焊缝区硬度最低，而由于 θ 相的重新固溶析出，热影响区硬度较焊缝区有明显提高。

关键词：2519 高强铝合金；双丝 GMAW 焊接；工艺
中图分类号：TG444 文献标识码：A 文章编号：0253－360X(2006)10－015－05

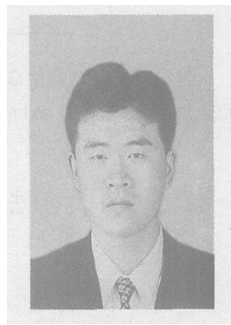

范成磊

## 0 序 言

2519 高强铝合金（Al-Cu-Mn 系）是一种新型装甲材料，具有较高的比强度和比刚度以及良好的加工和力学性能，尤为突出的是其在抗弹性能不低于原 7039 装甲铝合金前提下，在海水及盐雾环境下的抗应力腐蚀性能大大提高，是目前制造轻型装甲战车的理想材料[1,2]。铝合金装甲在生产过程中一般采用电弧焊的方法进行连接，但是焊接过程中存在热裂倾向大、气孔敏感性高等问题，同时 2519 铝合金对焊接热输入比较敏感，工艺规范控制不当接头组织会发生变化，影响焊缝及热影响区的性能，进而严重降低了焊接结构件的总体强度和使用寿命，这些特点使得 2519 铝合金在国内目前还没有得到推广和应用。炮塔装甲构件通常都比较厚大（厚度达 20～80 mm），用常规弧焊方法进行连接，生产效率非常低下。双丝 GMAW 焊方法是近年来新推出的焊接方法，同普通单丝 GMAW 焊相比，双丝焊具有焊接效率高、热影响区小、低飞溅和低气孔率等优点，尤其适用于厚板铝合金装甲的生产。

文中针对 2519 高强铝合金厚板双丝 GMAW 焊接工艺进行探索和研究，确保获得良好的焊缝成形和接头性能，为国防工业提供技术支持。

收稿日期：2006－03－21
基金项目：国家 863 高科技资助项目（2002AA305402）

## 1 双丝 GMAW 焊接原理

双丝 GMAW 焊接原理如图 1 所示[3]，两根焊丝通过一个特别设计的焊枪按一定的角度送入到同一个熔池中，两根焊丝由各自的电源供电，送丝速度、脉冲电压、脉冲频率、基值电流、脉冲时间等参数都可独立调节，电弧控制非常灵活。双丝 GMAW 焊由两根焊丝同时熔化、处于同一个熔池中，二者互相加热，最大限度的减少了热量损失，提高了熔敷速度和生产效率。

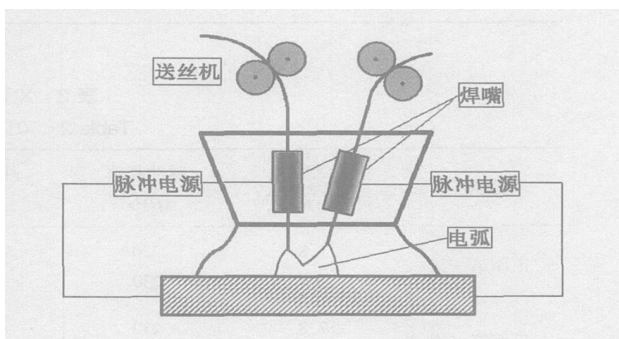


图 1 双丝 GMAW 焊接原理图
Fig. 1 Schematic diagram of double-wire GMAW welding

双丝 GMAW 焊接时前、后丝对焊缝成形有着不同的影响，如图 2 所示，焊接时前丝与焊件垂直且使用较大的电流和较低的电压，形成较大的熔深（S）；后

丝与前丝成一定夹角，保持相对较小的电流和略高的电弧电压，从而达到提高焊缝熔宽(C)的目的。因此焊接时应根据两根焊丝的不同作用选择合适的参数。

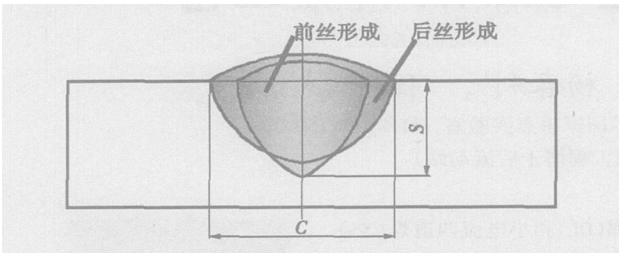


图 2 前后丝对双丝 GMAW 焊缝成形的影响

Fig. 2 Influence of front and rear wire to appearance of weld

对坡口和焊丝进行清理，去除沾附的杂质和油污。

根据焊接层数和电流的不同，共进行了三种工艺试验，分别命名为大电流两道焊(DL)、小电流四道焊(XS)和大电流四道焊(DS)。首先介绍 DL 和 XS 工艺试验，表 1，表 2 分别是 DL、XS 工艺试验的焊接工艺参数。

DL 焊接时，正反各焊一道，焊接背面焊道时先进行清根，并适当增加焊接电流而降低电压，这样可以进一步增大反面熔深，减少根部可能出现的缺陷。XS 焊接顺序为先焊正面第一道，反面清根后焊第一道，再焊反面第二道，最后焊正面第二道，这样有利于减少焊接变形。

## 2 试验材料及方法

试验材料是 2519 T－87 高强铝合金，采用平板对接方式，每块试板的尺寸为 500 mm× 120 mm× 20 mm，试件板边开对称双 U 形坡口，坡口角度为 70°，具体形状参数如图 3 所示。在焊第一道焊缝时为避免焊穿，焊缝背面使用与坡口形状一致的紫铜垫板。焊接时选用美国产ER2319铝合金焊丝，焊接前应

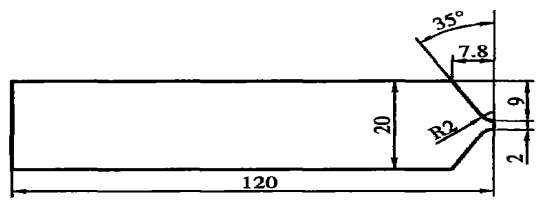


图 3 试板坡口形式 (mm)

Fig. 3 Groove of weldment

表 1 DL 焊接工艺参数

Table 1 DL welding conditions

| 焊接顺序 | 送丝速度 $v_1$/(m·min$^{-1}$) | 脉冲频率 $f$/Hz | 脉冲电压 $U$/V | 脉冲时间 $t$/ms | 基值电流 $I$/A | 焊接速度 $v$/(mm·min$^{-1}$) |
|---|---|---|---|---|---|---|
| 正面 | 10.0 | 230 | 25.0 | 2.2 | 100 | 415 |
| | 7.5 | 200 | 26.0 | 2.0 | 100 | |
| 反面 | 10.5 | 230 | 24.0 | 2.2 | 100 | 415 |
| | 7.5 | 200 | 25.5 | 2.0 | 100 | |

表 2 XS 焊接工艺参数

Table 2 XS welding conditions

| 焊接顺序 | 送丝速度 $v_1$/(m·min$^{-1}$) | 脉冲频率 $f$/Hz | 脉冲电压 $U$/V | 脉冲时间 $t$/ms | 基值电流 $I$/A | 焊接速度 $v$/(mm·min$^{-1}$) |
|---|---|---|---|---|---|---|
| 正面第一道 | 7.8 | 230 | 25.5 | 2.1 | 100 | 513 |
| | 7.0 | 230 | 26.0 | 2.1 | 100 | |
| 反面第一道 | 7.8 | 230 | 25.5 | 2.1 | 100 | 513 |
| | 7.0 | 230 | 26.0 | 2.1 | 100 | |
| 反面第二道 | 7.6 | 230 | 25.8 | 2.1 | 100 | 513 |
| | 7.0 | 230 | 26.5 | 2.1 | 100 | |
| 正面第二道 | 7.6 | 230 | 25.8 | 2.1 | 100 | 660 |
| | 7.0 | 230 | 26.5 | 2.1 | 100 | |

## 3　DL 及 XS 工艺试验结果及分析

图 4，图 5 分别是 DL 和 XS 焊缝表面成形情况，从图可以看出两种工艺条件下焊缝成形都非常良好，但 XS 焊缝表面更加细腻一些。从图 6 焊缝横截面图可知，DL 焊缝表面余高很小，甚至有些地方略有凹陷，这样的接头不能够适应对焊缝强度要求较高的装甲车炮塔结构件，从图 7 可以看出 XS 焊缝表面要比 DL 焊缝饱满。

由焊接接头拉伸试验结果（表 3）可以看出，DL 和 XS 焊接接头抗拉强度和伸长率与母材相比都显著降低，其中 XS 接头抗拉强度仅为 279.2 MPa，DL 接头的抗拉强度比 XS 接头高出 10.1 MPa，但仍不足母材的 60%（59.6%）。对两种接头进行 X 射线探伤发现，XS 焊缝区存在相对较多的气孔，这是由于 XS 焊接时每一道热输入量较小，焊接速度较快，熔池存在时间短，焊缝结晶时形成的气孔不能充分溢出熔池表面所致。正是这些气孔的存在使得接头的有效承载面积降低，导致抗拉强度和伸长率同时降低。

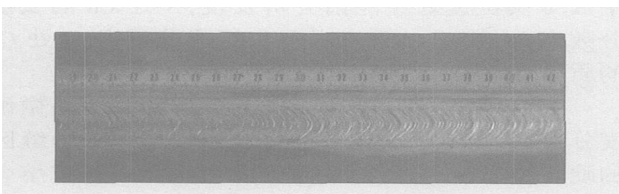

图 4　DL 焊缝表面成形

Fig. 4　Surface of DL weldment

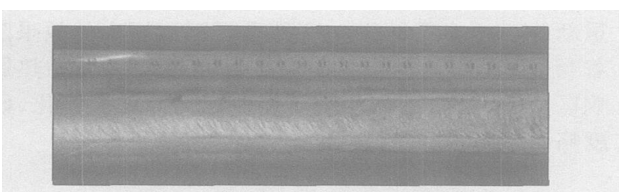

图 5　XS 焊缝表面成形

Fig. 5　Surface of XS weldment

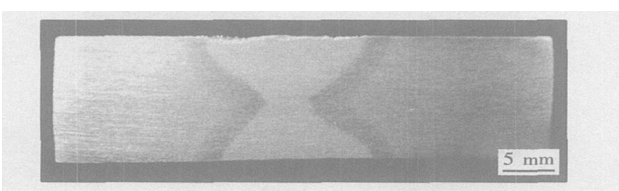


图 6　DL 焊缝截面图

Fig. 6　Cross section of DL weldment

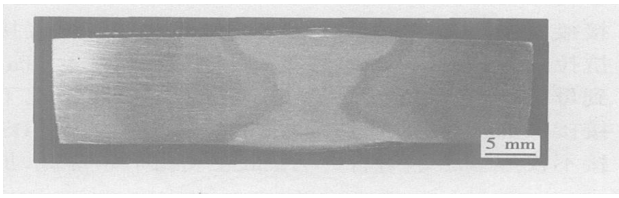


图 7　XS 焊缝截面图

Fig. 7　Cross section of XS weldment

从表 4 冲击试验结果可以看出，DL 焊缝金属的冲击韧度与母材相比显著降低，不足母材的 54%，而 XS 焊缝冲击韧度值为 16.91 J/cm$^2$，比 DL 焊缝高 37.2%。分析原因认为是 XS 焊时每一道所采用的热输入量比较低，熔敷金属高温停留时间短，冷却速度更快，焊缝晶粒相对较小，从而导致其冲击韧度值较高。

表 3　DL 和 XS 焊接接头拉伸试验结果

Table 3　Tensile test results of DL and XS welded joint

| 试样序号 | 抗拉强度 $R_m$/MPa | 屈服强度 $R_{eL}$/MPa | 断后伸长率（%） |
|---|---|---|---|
| 母材（轧制方向） | 484.7 | 442.2 | 18.4 |
| DL | 289.3 | 156.8 | 5.6 |
| XS | 279.2 | 173.6 | 4.8 |

表 4　DL 和 XS 焊接接头冲击试验结果

Table 4　Impact test results of DL and XS welded joint

| 试样序号 | 最大载荷 $P$/kN | 冲击吸收功 $A_{kv}$/J | 冲击韧度 $a_{kv}$/（J·cm$^{-2}$） |
|---|---|---|---|
| 母材（轧制方向） | 24.09 | 25.43 | 31.79 |
| DL | 5.31 | 9.85 | 12.32 |
| XS | 5.43 | 13.53 | 16.91 |

## 4　DS 焊接工艺优化及试验结果

通过对上述 DL、XS 两种工艺下焊接接头的对比分析表明，采用较大的焊接电流有利于增加焊缝熔深，增强对液态金属的搅拌，降低气孔和缩孔的数量，提高接头的抗拉强度；而采用多道焊时，由于每一道所使用的热输入量较小，焊缝冲击韧度较高且焊缝表面填充比较饱满。综合以上两种工艺的优点，提出一种优化的大电流四道焊（DS）的焊接工艺，其规范参数如表 5 所示，DS 焊接顺序与 XS 相同，但焊接电流和焊接速度要高得多。表 6 为 DS 焊

接接头拉伸性能数据，由此可以看出 DS 焊接接头抗拉强度比 DL 和 XS 都高，平均值为 296.4 MPa，达到母材的 61.2%，从表 6 还可以看出，DS 工艺下焊接接头的抗拉强度数据非常稳定。这是由于 DS 焊接不仅焊缝根部熔合充分，而且气孔率非常低，加之高的冷却速度下焊缝区晶粒细小均匀。

图 8 所示为 DL、XS 和 DS 三种焊接接头冲击韧度的对比，可见 DS 焊接接头的冲击韧度平均值为 13.25 J/cm$^2$，比 DL 焊接接头有所提高，达母材的 41.7%，但仍低于 XS 接头。

表 5 DS 焊接工艺参数

Table 5 DS welding conditions

| 焊接顺序 | 送丝速度 $v_f$/(m·min$^{-1}$) | 脉冲频率 $f$/Hz | 脉冲电压 $U$/V | 脉冲时间 $t$/ms | 基值电流 $I$/A | 焊接速度 $v$/(mm·min$^{-1}$) |
|---|---|---|---|---|---|---|
| 正面第一道 | 10.5 | 230 | 24.0 | 2.2 | 100 | 668 |
| | 7.0 | 200 | 26.0 | 2.0 | 100 | |
| 反面第一道 | 10.5 | 230 | 24.0 | 2.2 | 100 | 668 |
| | 7.0 | 200 | 26.0 | 2.0 | 100 | |
| 反面第二道 | 10.0 | 230 | 24.5 | 2.2 | 100 | 534 |
| | 7.0 | 200 | 26.8 | 2.0 | 100 | |
| 正面第二道 | 10.0 | 230 | 24.5 | 2.2 | 100 | 534 |
| | 7.0 | 200 | 26.8 | 2.0 | 100 | |

表 6 DS 焊接接头拉伸试验数据

Table 6 Tensile test results of DS welded joint

| 试样序号 | 抗拉强度 $R_m$/MPa | 屈服强度 $R_{eL}$/MPa | 断后伸长率 $A$(%) |
|---|---|---|---|
| 1 | 297.3 | 172.5 | 6.2 |
| 2 | 296.9 | 173.7 | 6.5 |
| 3 | 295.0 | 174.0 | 5.4 |
| 平均值 | 296.4 | 173.4 | 6.0 |

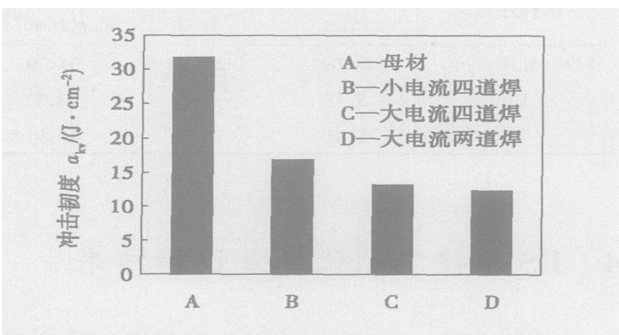


图 8 DL 和 XS 及 DS 三种接头冲击韧度对比

Fig. 8 Impact toughness of DL, XS and DS welded joint

## 5 2519 铝合金焊缝区组织及硬度分析

2519 铝合金熔池在冷却过程中富 Al 的 α 相先从液相中结晶出来，Cu 原子大多被排挤到剩余的液相当中。当温度的降低达到共晶线附近时，剩余的液相由于 Cu 的含量越来越多，达到共晶成分时，开始析出共晶组织(θ 相)。图 9 为 DS 焊缝区组织，图中 A，B 两位置处经能谱分析发现，A 处 Cu 的质量分数为 24.57%，大致与共晶组织成分相当；B 处 Cu 的质量分数为 6.68%，与 α 相的成分比较接近。

图 10 为大电流四道焊规范下焊接接头显微硬度分布，从图中可以看出在整个焊接接头中焊缝区的硬度最低，整个焊缝区硬度差别不大。靠近熔合线的热影响区硬度明显升高，这是热影响区靠近焊缝的部分金属在高温状态下从母材中析出的 θ 相的过渡相重新固溶到 α 相当中，而在随后冷却过程中重新弥散析出的结果。这种重新固溶析出的效果随着与焊缝距离的增加而减弱，因此靠近母材的热影响区表现为过时效状态[4,5]，使得这里发生软化，硬度略有降低。

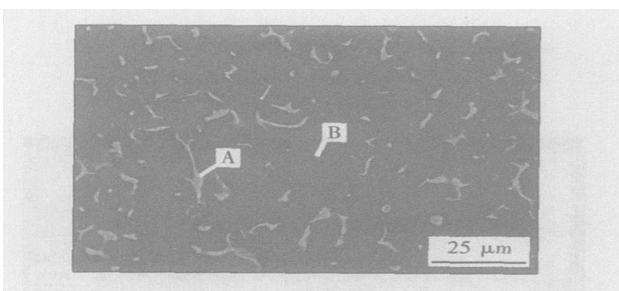


图 9 DS 焊缝区组织

Fig. 9 Metallographic structure of DS weld bead

[下转第 22 页]

种变化趋势。

## 4 结 论

(1) 母材的断裂应变对焊接接头的 J 积分有明显的影响。随着母材区断裂应变的减小，焊缝裂纹尖端韧带区的塑性应变及 J 积分断裂参量均有明显的提高。表明母材的损伤程度增加会导致焊接接头裂纹扩展驱动力的增加。

(2) 随着接头强度匹配比 $M$ 的降低(或母材屈服强度的升高)，母材区断裂应变对焊缝区塑性应变及 J 积分断裂参量的影响作用减小。这是由于应变向焊缝区集中的原因。

参考文献：


[1] Zhang J X, Shi Y W, Tu M J. Studies on the fracture mechanics parameters of weldment with mechanical heterogeneity[J]. Engineering Fracture Mechanics, 1989, 34(5/6): 1041—1050.

[2] Zhang M, Shi Y W, Zhang X P. Influence of strength mis-matching on crack driving force and failure assessment curve of weldment[J]. International Journal of Pressure Vessels and Piping, 1997, 70(1): 33—41.

[3] Tang W, Shi Y W. Influence of strength matching and crack depth on fracture toughness of welded joints[J]. Engineering Fracture Mechanics, 1995, 51(4): 649—659.

[4] Kachanov L M. Rupture time under creep conditions[J]. International Journal of Fracture, 1999, 97(1/4): 11—18.

[5] Lemaitre J. A continuous damage mechanics model for ductile fracture [J]. Journal of Engineering Materials and Technology, 1985, 107(1): 83—89.

[6] Chaboche J L. Contiuum damage mechanics: part I—general concepts [J]. Journal of Applied Mechanics, 1988, 55(1): 59—64.

[7] Hval M, Thaulow C, Lange J H, *et al*. Numerical modeling of ductile fracture behavior in aluminum weldments[J]. Welding Journal, 1998, 77(5): 208s—217s.

[8] Wang T J. A continuum damage model for ductile fracture of weld heat affected zone[J], Engineering Fracture Mechanics, 1991, 40(6): 1075—1082.



作者简介：张建勋，男，1958 年 4 月出生，博士，教授，博士生导师。从事焊接科学与技术、精密激光加工、计算机模拟与仿真研究。发表学术论文 150 余篇。

Email：jxzhang@mail.xjtu.edu.cn


[上接第 18 页]

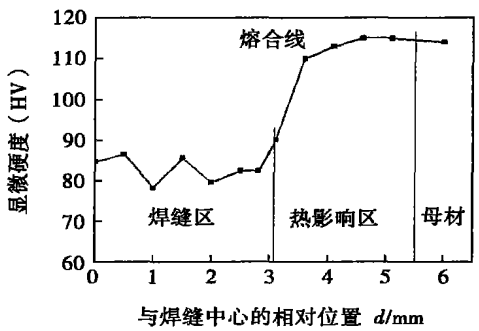


图 10 DS焊接接头硬度分布

Fig. 10 Hardness of DS welded joint

## 6 结 论

(1) DL 及 XS 焊接工艺焊缝成形良好，XS 焊缝成形更加饱满；两种工艺条件下焊接接头抗拉强度较低，都不足母材的 60%，但 DL 焊接接头的抗拉强度比 XS 高；两种焊缝处的冲击韧度都比母材低很多，XS 焊缝冲击韧度比 DL 焊缝高 37.2%。

(2) 综合 DL 和 XS 焊接的优点，提出了优化的 DS 焊接规范，其焊接接头抗拉强度达到母材的 61.2%。焊缝区冲击韧度也较 DL 情况有明显提高。

(3) DS 焊缝区组织主要是 α 相和弥散分布的共晶组织；对接头进行硬度测试发现，焊缝区硬度最低，而由于 θ 相的重新固溶析出，热影响区硬度较焊缝区有明显提高。

参考文献：


[1] Fisher J J, Kramer L S, Pickens J R. Aluminum alloy 2519 in military vehicles[J]. Advanced Materials and Processes, 2002, 160(9): 43—46.

[2] Devincent S M, Devletian J H. Weld properties of the newly developed 2519—T87 aluminum armor alloy [J]. Welding Journal, 1988, 67(7): 33—43.

[3] 魏占静. 先进的TANDEM 焊接技术[J]. 现代制造, 2003, (12): 32—33.

[4] Janaki G D, Murugesan R, Sundaresan S. Fusion zone grain refinement in aluminum alloy weld through magnetic arc oscillation and its effect on tensile behavior [J]. Material Engineering Perform, 1999, 8(5): 513—520.

[5] Gutierrez A, Lippold J C. A proposed mechanism for equiaxed grain formation along the fusion boundary in aluminum-copper-lithium alloy [J]. Welding Journal, 1998, (3): 123—132.



作者简介：范成磊，男，1976 年 6 月出生，博士后研究人员，讲师。主要研究方向为焊接过程控制及高效焊接，发表论文 20 余篇。

Email：fclwh@hit.edu.cn

# MAIN TOPICS, ABSTRACTS & KEY WORDS

**Microstructure of LY12 aluminium alloy welded joint of friction plug welding** LUAN Guo-hong, JI Ya-juan, DONG Chun-lin, MA Xiang-sheng (China FSW Center, Beijing Aeronautical Manufacturing Technology Research Institute, Beijing 100024, China). p1—3

**Abstract**: Friction plug welding is a novel solid state joining and repairing process. Based on the introduction of basic principle of friction plug welding process, preliminary studies on microstructure and hardness distribution of friction plug welded joint were carried out. It is shown that five zones could be easily identified in LY12 joint, i. e. the base metal, plastic zone Ⅰ, the transition zone between base metal and plastic zone Ⅰ, plastic zone Ⅱ, the transition zone between plastic zone Ⅰ and plastic zone Ⅱ. Drastic material deformation and metal flow occurr in plastic zone Ⅰ and Ⅱ, but these two zones have different flow patterns. Hardness of the joint decreases from the base metal and reaches a minimum in the plastic zone Ⅰ, and then gradually increases to a stable level in plastic zone Ⅱ which equal to the base metal. The other side of the joint has the same trend of hardness distribution.

**Key words**: LY12 aluminum alloy; friction plug welding; microstructure; hardness

**Analysis on electromagnetic force in resistance spot welding** WU Pei, MA Yan-hua, HAN Bao-sheng, LI Fen-rong (Inner Mongolia Agricultural University, Huhhot 010018, China). p4—6

**Abstract**: In resistance spot welding, a strong magnetic field is generated due to a high current applied. A theoretical analysis on electromagnetic force caused in the process of resistance spot welding was carried out based on stationary machines by simplifying the electrode arms and electrodes as electric conductors, and the electromagnetic force was measured by means of a middle-frequency DC machine. The results indicate that the electromagnetic force has an effect on reduction of the electrode force, i. e. counteracting the electrode force. The electromagnetic force is mainly affected by the welding current and electrode-arm open depth. It is direct proportional to the square of the welding current and inverse proportional to the electrode-arm open depth. Therefore, the effect of electromagnetic force must be considered when the electrode force is set or measured in the real production.

**Key words**: resistance spot welding; electromagnetic force; electrode force

**Ultrasonic TOFD technique and image enhancemetn based on synthetin aperture fousing techinque** GANG Tie, CHI Da-zhao, YUAN Yuan (State Key Lab of Advanced Welding Production Technology, Harbin Institute of Technology, Harbin 150001, China). p7—10

**Abstract**: An ultrasonic TOFD (time of flight diffraction) B-scan image was processed in order to accurately locate crack tip in heavy aluminum butt weld. SAFT (synthetic aperture focusing technique) was introduced for improving lateral resolution of the image. According to the geometric relation between the probes and crack tip, an algorithmic model for SAFT processing was founded and SAFT reconstruted image was obtained. Linearization was proposed in order to enhance time resolution of the image before SAFT processing, and a novel technique named as L-SAFT (linearization-SAFT) was developed for ultrasonic TOFD B-scan image reconstruction. The results show that the technique can enhance resolution of the image effectively. Both lateral and vertical location of the crack tip in the specimen can be measured rapidly and accurately with this techinque, which contribute to precise locating and sizing of defect.

**Key words**: ultrasonic time of flight diffraction; crack; linearization; synthetic aperture focusing technique

**Welding process parameter Web publish system based on internet** WANG Ke-hong, YANG Yan, WANG Bo (Materials department, Nanjing University Science&Technology, Nanjing 210094, China). p11—14

**Abstract**: The welding process parameters system was built to solue the problem of the welding data acquisition and managing in far distance welding, and its software system and hardware system had also been designed. It can obtain lots of welding process information, such as welders, welding product, welds. The welding process information are acquired by several acquisition model and channel, then the software model was designed to acquire welding current and voltage and display their waveforms in the computer screen. At last the welding process parameter web publishing system is accomplished.

**Key words**: welding parameters; data acquisition; gas metal arc welding

**Tandem GMAW procedure of 2519 high strength aluminum alloy** FAN Cheng-lei[1,2], LIANG Ying-chun[2], YANG Chun-li[1], CHENG Shi-jun[1] (1. State Key Laboratory of Advanced Welding Production Technology 2. Mechanical Engineering Mobile Postdoctoral Center; Harbin Institute of Technology, Harbin 150001, China). p15—18, 22

**Abstract**: The relationship between mechanical properties and weld appearance of the joints by the two-pass welding with large current (DL) and the four-pass welding with small current (XS) were investigated in tandem GMAW of 20mm thick 2519 aluminum alloy plate. The results show the tensile strength of both joints are less than 60% of that of the base metals, and the tensile strength and elongation percentage of the DL joints are larger than those of the XS joints, but the impact toughness of the DL joints is smaller. Based on the merits of the above two process, a new process named four-

pass welding with large current (DS) was puts forward. The experimental results show the tensile strength of the DS joint is up to 296.4 MPa, equivalent to 61.2% of that of base metal and the impact toughness of the DS joint improved simultaneously. The DS weld zone is composed of α phase and eutectic structure grains. Hardness of the weld is the lowest on the whole weldment, and the hardness of the HAZ is higher because the θ phase dissolve and separate out renewedly.

**Key words**: 2519 high strength aluminum alloy; tandem gas metal arc welding; procedure

**Numerical simulation on fracture mechanics parameters of welded joint with damage** ZHANG Jian-xun, LI Ji-hong(State Key Laboratory for Mechanical Behavior of Materials, Xi'an Jiaotong University, Xi'an 710049, China). p19—22

**Abstract**: The fracture mechanics parameters of welded joint with damage were numerically simulated with fully coupled strain and damage elastic-plastic finite element method for center-cracked specimens with welded joint. The results show that the rupture strain of base metal has large effects on the fracture behavior of crack in weld metal. If mechanical parameters of weld metal are kept constant, the plastic strain along the ligament and the J-integral increase with the decrease of the rupture strain of base metal for any strength matching ratio. With the decrease of strength matching ratio (viz. the increasing of the strength of base metal), the effect of the rupture strain of base metal on the J-integral is weaken gradually.

**Key words**: damage; welded joint; fracture mechanics parameters; finite element method

**Discussion on determination of J-integral and comparison of different test standards** DENG Cai-yan, ZHANG Yu-feng, HUO Li-xing(School of Materials Science and Engineering, Tianjin University, Tianjin 300072, China). p23—25, 32

**Abstract**: According to different fracture toughness test standard, J-Resistance curve tests were conducted at -5℃ in welded joints of X56 pipeline steel in the multiple specimen method and the test result were compared. According to the double P-V curves of each weld metal and heat affected zone specimen obtained from the two notch opening displacement the load-line displacement and the value of J were calculated. Finally, the best fited curve was determined the valid data points according to GB2038-91 and BS7448, respectively. The result indicates that BS7448 is superior to GB2038-91 on blunt line, exclusion lines and so on. J-Resistance curves and $J_{0.2}$ was obtained. But there are no valid data points according to GB2038-91 and no further calculation.

**Key words**: J integral; resistance curve; blunt line

**A numerical calculation on contact surface stress field of metals explosive welding** XIE Fei-hong[1,2], LUO Guan-wei[3], WANG Xu-guang[4](1. School of Civil Engineering, Lanzhou Jiaotong University, Lanzhou 730070, China; 2. School of Civil and Environmental Engineering, Beijing University of Science and Technology, Beijing 100083, China; 3. College of Mechanical-Electronics Engineering, Lanzhou Jiaotong University, Lanzhou 730070, China; 4. Beijing General Research Institute of Mining and Metallurgy, Beijing 100044, China). p26—28, 93

**Abstract**: The impact pressure produced by explosive detonation is essential condition of the base plate and cladding plate coalescence for metal explosion welding. Based on Rayleigh—Ritz calculating model and elasticity variation principle, elasticity problem is considered as functional arrest ental equation, and boundary condition of the problem is given. Differential equation and corresponding boundary condition are derived. Instantaneous stress field at impact points was calculated, and analog calculating of different collision angles and impact pressures were carried out. Basic law of stress field distribution at impact points was found. The calculating stress field distribution law can be applied to evaluation and guidance of practical engineering.

**Key words**: explosive welding; calculation model; impact pressure; stress field; value calculation

**Agglomerated alkali flux for submerged arc welding of high strength-toughness steel X80** ZHANG Min, YAO Cheng-wu, LIU Bin, LI Ji-hong(School of Material Science and Engineering, Xi'an University of Technology, Xi'an 710048, China). p29—32

**Abstract**: Through analyzing acicular ferrite nucleating mechanism in the weld metal of the high strength low-alloy structural steel (HSLA), a submerged arc welding agglomerated flux with the $CaF_2$-MgO-$Al_2O_3$-MnO-$TiO_2$-$B_2O_3$ fluorine was developed by using alkali flux system. The results indicate that the existence of MnO in the flux benefits the transition of Mn to weld metal, and brings down the γ→α transformation temperature, thus high temperature ferrite production is held down, but the acicular ferrite increases in the weld metal. Because the Pcm of weld metal is higher, the austenite grain is thinner as-welded in air cooling condition. However, a excessive content of MnO in the flux will lead to the excessive Mn in the weld metal and a too low γ→α transform temperature. Thereby, the austenite grain boundaries cannot be decorated by allotriomorphic ferrite, thus the austenite grain boundary increases, which make more bainite nucleation site being produced. It is disadvantageous to the intragranularly nucleated acicular ferrite. In addition, the rare-earth element has some contributions to enhance the acicular ferrite content in the weld metal.

**Key words**: agglomerated flux; strength and toughness; acicular ferrite; intragranular nucleation; phase transformation temperature

**$CO_2$ laser welding process of aluminum alloy with filler powder** CHEN Kai, XIAO Rong-shi, ZHANG Seng-hai, ZUO Tie-chuan(College of Laser Engineering, National Center of Laser Technology, Beijing University of Technology, Beijing 100022, China). p33—36

**Abstract**: The experiments were carried out with $CO_2$ (slab) laser. The five stages of the inter actions between laser and powder in the laser welding with powder were analyzed. The influences of the filler metal powder on the laser power density threshold value, weld formation and process stability were studied during $CO_2$ laser